Pioneer. Adv. Mater. 2026, 2(1): 1-12 DOI: 10.48308/piadm.2026.245487.1029

Shahid Beheshti University

Pioneering Advances in Materials

Journal homepage: http://pioneering.sbu.ac.ir

ISSN: 3115-7114

Original Research

Investigating the Effect of High-Repetition-RateFemtosecond Laser Parameters on Heat Accumulation in Bulk Fused Silica

Zahra Norouzi Benis , Atoosa Sadat Arabanian* , Somayeh Najafi , Reza Massudi

Laser and Plasma Research Institute, Shahid Beheshti University, Tehran, Iran

*a_arabanian@sbu.ac.ir

Article info:

Article history:

Received: 20/07/2026
Accepted: 11/08/ 2026

Keywords:
Femtosecond laser processing, Heat accumulation, repetition rate, Struc-tural modification

Abstract

Femtosecond laser irradiation enables modification of transparent materials and is used to fabricate optical waveguides and optofluidic devices. In this study, the propagation of 50 fs laser pulses at 800 nm within fused silica was modeled using the nonlinear Schrodinger equation coupled with a rate equation for free-electron density. Because fused silica exhibits negligible linear absorption at 800 nm, energy deposition was attributed to nonlinear ionization and subsequent absorption by free electrons. The deposited-energy distribution was then used as the heat source in a non-Fourier heat-conduction model to investigate temperature evolution during repeated irradiation. The effects of repetition rate, pulse energy, and scanning speed on heat accumulation were examined. The results show that repeated irradiation produces temperature increases even when the deposited energy is insufficient to reach the softening or melting range. During scanning, temperature approaches a quasi-steady state after several pulses and then changes along the scan path. Increasing pulse energy raises the temperature, broadens the temperature distribution, and prolongs cooling time. Increasing the repetition rate from 100 kHz to 1 MHz produces a more symmetric temperature distribution and extends affected region beyond the focal volume. At 100 kHz, increasing pulse energy from 0.3 to 1 μJ increases temperature, with limited expansion of the affected region. Higher repetition rates enhance heat accumulation and raise the quasi-steady temperature, whereas higher scanning speeds reduce interaction time and accumulated heat. When the number of pulses per point remains constant, increasing repetition rate and scanning speed shortens stabilization time while increasing accumulated temperature.

1. Introduction

Direct laser writing techniques could serve as a viable alternative to conventional photolithography methods, which typically require a cleanroom environment and expensive equipment. They offer reduced complexity and cost for producing optical devices and integrated circuits. Direct laser writing has been demonstrated using continuous-wave, nanosecond, and femtosecond lasers. Among these methods, writing with femtosecond lasers offers several potential advantages.

During the interaction of femtosecond pulses with matter, nonlinear processes can occur even in materials that are transparent at the laser wavelength, making this method applicable to different types of samples. Because the duration of femtosecond pulses is several orders of magnitude shorter than that of conventional laser pulses, their peak power is very high despite their relatively low energy. For a given pulse energy and focal geometry, the pulse duration determines the peak intensity and therefore strongly affects nonlinear ionization, plasma generation, and the amount of energy deposited in the material. This combination enables nonlinear energy deposition inside transparent materials.

Although fused silica has negligible linear absorption at 800 nm, the high intensity reached near the focus can generate free electrons through nonlinear ionization. The electron population can then absorb additional laser

energy, and the deposited energy is transferred to the lattice, leading to localized heating and, under suitable conditions, permanent structural modification. Due to the nonlinear nature of laser pulse absorption, the structural changes created inside the transparent material remain geometrically confined to the focal region. This feature reduces lateral thermal damage near the focal point, resulting in a smaller heat-affected zone.

Another advantage of this method is the ability to control and adjust processing parameters such as pulse duration, wavelength, repetition rate, pulse energy, beam polarization, focal geometry, and scanning speed to create a variety of structures in different samples, including multilayer samples. With the rapid development of femtosecond lasers in the 1990s, the first experiment on laser-induced breakdown in a fused silica sample was performed in 1994 [2], followed by the creation of the first optical waveguide structures written by a femtosecond laser inside bulk glass in 1996 [3].

In recent decades, with advancements in the manufacturing technology of this type of laser, as well as increasing attention to micro-optical and microelectronic integrated circuits, significant progress has been made in the field of femtosecond laser processing. High-quality optical waveguides and various optical elements are inscribed within the bulk of transparent materials for the fabrication of diverse microfluidic, optofluidic, and photonic devices [4, 5, 6, 7, 8, 9, 10, 11].

The mechanisms of structural modification vary with the laser-processing parameters and the characteristics of the materials, necessitating comprehensive studies to predict these changes under various conditions. Such studies can help identify suitable processing parameters for different applications and improve the understanding of laser-induced structural modification.

In certain micromachining applications, multiple pulses, often numbering in the thousands, are directed at a specific point within the sample, necessitating consideration of thermal accumulation effects. Under certain conditions, it has been observed that the size of the modified region increases with the number of pulses applied to a single point [3, 12, 13, 14]. However, in some other cases, it has been observed that, for certain repetition rates and specified pulse energies, increasing the number of pulses does not alter the size of the modified region, which remains constant [15].

Some researchers have reported the phenomenon of incubation (the gradual creation of structural changes) in surface machining. In this phenomenon, the damage threshold decreases after several pulses compared with a single pulse because of thermal accumulation [16]. However, this phenomenon has been studied less extensively in the bulk of transparent materials.

On the other hand, many experimental studies have been conducted to obtain the optimal combination of micromachining parameters in bulk fused silica glass. In 2003, Schaffer and his colleagues investigated the deposition of thermal energy in bulk transparent material in the high-repetition-rate regime using a femtosecond laser oscillator with a pulse duration of 30 fs, a wavelength of 800 nm, and a repetition rate of 25 MHz [17]. In addition, they showed that the laser focal area, acting as a point heat source in bulk transparent material, leads to a change in the refractive index due to local melting and solidification of that area. The amount of thermal energy stored in the focal region can be controlled with nanojoule precision at low pulse energies by adjusting the number of incident pulses at each point. No other micromachining techniques can provide such precision in depositing thermal energy at micrometer dimensions within bulk material. They also showed that the micromachining speed of femtosecond laser oscillator systems with repetition rates in the megahertz range, due to their high pulse rate, is two to three times higher than that of amplified femtosecond laser systems with repetition rates in the kHz range.

Sakakura et al. showed that the temperature of the focal region of borosilicate glass irradiated with a femtosecond laser pulse with a duration of 220 fs decreased to less than 100°C within 10 μs after the end of the pulse, implying that thermal accumulation becomes evident at pulse repetition rates greater than 100 kHz [18]. However, practical limitations make it difficult to determine a suitable combination of processing parameters through experiments alone.

To solve this problem, many numerical models have been presented to investigate the effects of thermal accumulation and structural changes in dielectrics under various conditions involving ultrashort pulses with high repetition rates. In these studies, thermal models have been widely used to calculate time-dependent thermal distributions and determine the shape and size of the heat-affected area. In these models, as an approximation, the heat source is considered a Gaussian function similar to the intensity distribution of the incident field [19, 20, 21, 22, 23].

In 2014, Miyamoto et al. presented a numerical model to determine the absorbed-energy intensity distribution, nonlinear absorption, and temperature distribution in the focal region for different repetition rates, scan speeds, and pulse energies in glass irradiated with femtosecond and picosecond laser pulses. They showed experimentally that the cross-section has a dual structure consisting of a teardrop-shaped inner structure and an elliptical outer structure [24]. They also showed that nonlinear absorption increases in the high-repetition-rate regime. Furthermore, the melt zone created in the focal zone due to thermal accumulation, surrounded by a transparent

solid matrix, enables crack-free welding inside glass by preventing shrinkage stress. Meanwhile, in the welding of glass using the conventional method with continuous-wave lasers, the formation of cracks is inevitable due to the stress created during the cooling process.

In 2021, Shen and his colleagues presented another numerical model to calculate the size of the modification region in glass welding for different picosecond laser parameters, including pulse energy, scan speed, and repetition rate [25]. They established a three-dimensional steady-state model for beam propagation with a transient ionization model to estimate the free-electron density produced by a single laser pulse. They then employed a heat-accumulation model for multiple laser pulses to describe the thermal distribution in the focal area under different scanning conditions. Therefore, they calculated the shape and size of the cross-section of the written lines. The results of their model agreed well with the results of the experimental tests.

Although the nonlinear processes of plasma formation and energy deposition in a transparent dielectric bulk irradiated with an ultrashort single pulse have been numerically investigated, there are few theoretical and numerical studies describing the structural changes resulting from an ultrashort pulse train with a high repetition rate. As mentioned above, thermal accumulation and diffusion can change the refractive index in the focal region, and these changes depend on micromachining parameters such as scanning speed, pulse energy, repetition rate, and focusing conditions. However, the exact dependence of structural changes on the micromachining parameters is not fully understood. To achieve optimal parameters for fabricating micro-optical devices useful for industrial applications, further studies of these parameters are required.

In the present simulations, 50 fs pulses at a wavelength of 800 nm were focused inside bulk fused silica. Unlike models that prescribe a Gaussian heat source, the deposited-energy distribution was calculated by solving the nonlinear Schrodinger equation coupled with a rate equation for the free-electron density. This approach accounts for nonlinear pulse propagation, plasma generation, and laser-energy absorption within the material. The resulting deposited-energy distribution was then used in a non-Fourier heat-conduction model to calculate the temperature evolution under successive pulses. The effects of pulse energy, repetition rate, and scanning speed were examined under fixed focusing conditions, and an optimal combination of these parameters was obtained.

2. Principles and theory

This section presents the equations describing nonlinear pulse propagation, plasma generation, energy deposition, and heat diffusion in bulk fused silica. Pulse propagation in a transparent material is described by the nonlinear Schrodinger equation coupled with the plasma equation. Under the slowly varying envelope approximation, the nonlinear Schrodinger equation is written in cylindrical coordinates as follows:

$$\begin{aligned}\frac{\partial E}{\partial z} &= \frac{i}{2k_0}\left(\frac{\partial^2}{\partial r^2}+\frac{1}{r}\frac{\partial}{\partial r}\right)E \\ &\quad -\frac{ik''}{2}\frac{\partial^2 E}{\partial t^2}+\frac{ik_0 n_{nl}}{n_0}|E|^2E \\ &\quad -\frac{\sigma}{2}(1+i\omega_0\tau_c)\rho_e E-\frac{\beta^{(m)}}{2}|E|^{2m-2}\end{aligned} \tag{1}$$

where $E(r,z,t)$ is the slowly varying envelope of the electric field, r is the radial coordinate, z is the propagation direction, and t is the retarded time. The term on the left-hand side describes the evolution of the pulse envelope along the propagation direction. On the right-hand side, the first term accounts for transverse diffraction of the beam, while the second term describes temporal pulse broadening caused by group-velocity dispersion. The third term represents the optical Kerr response of the material and accounts for self-focusing and self-phase modulation. The fourth term describes the effect of the free-electron plasma on the propagating laser pulse. Its real part represents absorption of laser energy by free electrons through inverse Bremsstrahlung, whereas its imaginary part accounts for the plasma-induced change in the refractive index and the resulting defocusing of the beam. The last term represents the loss of laser energy through multiphoton absorption.

Here, k_0 is the wave number at the central laser frequency, and n_0, n_2 are the linear and nonlinear refractive indices of fused silica, respectively. Here, $n_0$is the linear refractive index of fused silica at the laser wavelength of 800 nm. The parameter β_m denotes the multiphoton absorption coefficient, σ is the inverse-Bremsstrahlung absorption cross-section, and τ_c is the characteristic collision time of the laser-generated free electrons with the surrounding lattice and is typically on the order of a few femtoseconds. The free-electron density ρ_e, which appears in Eq. (1), is obtained from the following plasma rate equation:

$$\frac{\partial \rho_e}{\partial t}=\frac{\sigma}{E_g}I\rho_e+\sigma_m I^m\rho_{nt}-\frac{\rho_e}{\tau_{tr}} \tag{2}$$

Here E_g is the band gap and $I=\frac{1}{2}\varepsilon_0 n_0|E|^2$ shows the pulse intensity. The first and second terms on the right side of the above equation, respectively, represent the effect of avalanche and multiphoton ionizations in

increasing plasma density, and the third term represents the effect of electron-hole recombination with characteristic time of τ_{tr} in reducing plasma density. Temporal and spatial changes in the slowly varying electric field amplitude during pulse propagation inside the dielectric material and the electron density changes produced in the material in this interaction are obtained by numerically solving the coupled Eqs. (1) and (2). Then, it is possible to calculate the energy density deposited in the focal region by calculating the time integral of the power absorbed in the sample, due to the phenomena of multiphoton ionization and inverse Bremsstrahlung absorption. This time integral is written as follows:

$$\begin{aligned}\Delta E &= \int_0^{\tau_p} ((U_m W_{MPI}\rho_{nt}) + E_g Q_{br}\rho_e)dt \\ &= \int_0^{\tau_p} ((mh\omega_0\sigma_m I^m\rho_{nt}) + \sigma I\rho_e)dt\end{aligned} \tag{3}$$

In this expression, $W_{MPI} = \sigma_m I^m$ is the rate of multiphoton ionization, $U_m = m\hbar\omega_0$ is the energy of m photons, and $Q = \sigma I/Eg$ is the rate of inverse Bremsstrahlung absorption. Eq. (3) gives the energy density deposited through multiphoton ionization and inverse-Bremsstrahlung absorption. Although fused silica has negligible linear absorption at 800 nm, the high intensity of the focused 50 fs pulse generates a free-electron population through nonlinear ionization. These electrons absorb additional energy from the laser field, and the deposited electronic energy is then transferred to the lattice through electron-phonon interactions. This transfer produces a local rise in the lattice temperature on a picosecond timescale. When successive pulses arrive before the deposited heat has fully diffused from the focal region, the residual temperature increases from pulse to pulse, resulting in thermal accumulation. According to the classical theory of Fourier heat conduction, it is possible to calculate the thermal diffusion and time evolution of the dielectric temperature in the focal region. Based on this theory, the heat flux is proportional to the thermal gradient. Here, the propagation speed of the thermal wave is considered infinite. While the Fourier theory of heat diffusion is valid in most engineering problems, in our problem the extreme thermal gradient in short time scales cannot be justified based on this theory. A time delay equal to τ_q between the start of the heat flow process and the occurrence of the thermal gradient must be applied. Therefore, the non-Fourier thermal conductivity equation is used, in which the relationship between heat flux and thermal gradient is written as follows [26, 27]:

$$\rho C_p \frac{\partial T}{\partial t} + \rho C_p \tau_q \frac{\partial^2 T}{\partial t^2} = K\nabla^2 T \tag{4}$$

According to this equation, the temperature gradient at point r and time t leads to the heat flux at time $t + \tau_q$. In such a situation, the speed of the thermal wave is limited. This equation is used to calculate the spatio-temporal evolution of temperature in the hot zone that has been exposed to ultrashort pulse radiation. The initial temperature distribution used as the initial condition for the non-Fourier heat-conduction equation is then given by:

$$T_0(r.z) = \frac{E(r.z)}{\rho C_p} \tag{5}$$

where $\rho$and $C_p$are the material density and specific heat capacity, respectively. The initial temperature distribution calculated from calculating the Eq. (5) is then fed into the Eq. (4) as the initial condition of the equation. In this study, the spatio-thermal diffusion equation was solved using the Heat Diffusion module in COMSOL Multiphysics. Also, the lateral motion of the fused silica slab was made possible through moving the slab along the x axis as depicted in table 1. The various repetition rates were also applied using recurrently depositing the same initial temperature distribution inside the moving slab. A moving heat probe was deployed inside the very center of the focal region in order to investigate the thermal changes as the slab moves laterally along the track. In the simulations, fused silica is irradiated at a depth of 75 μm below the surface by focused femtosecond pulses. The pulse duration is 50 fs and the wavelength is 800 nm. The focal beam waist is 1 μm and the Rayleigh length is 11.2 μm. The optical and thermal constants used in solving the non-Fourier heat diffusion equation are listed in Table 1.

3. Results and discussion

a) Calculation of the initial temperature distribution produced by a single pulse

Initially, the temperature distribution within the bulk of fused silica is determined by solving the coupled nonlinear Schrodinger equation and plasma density equation following the incidence of a single pulse with a wavelength of 800 nm and a pulse duration of 50 fs. Fig. 1 illustrates the thermal distribution obtained from this model for pulse energies of 0.3, 0.5, and 1 μJ.

In the figures, to show the thermal distribution more clearly, the ratio of the r-axis to the z-axis is set to

Table 1. Optical and Thermal Constants of the Fused Silica Sample

Parameter	Value
Linear refractive index at 800 nm ($\mathbf{n_0}$)	1.45
Bandgap energy ($\mathbf{E_g}$)	9 eV
Specific heat capacity ($\mathbf{C_p}$)	703 J/kg·K
Thermal expansion coefficient (α)	55 $\times 10^{-8}$ 1/K
Density (ρ)	2190 kg/m^3
Thermal relaxation time (τ)	1 ps
Thermal conductivity ($\mathbf{K}$)	1.38 W/m·K

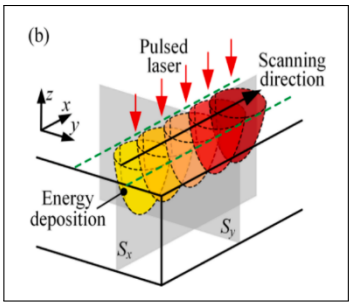

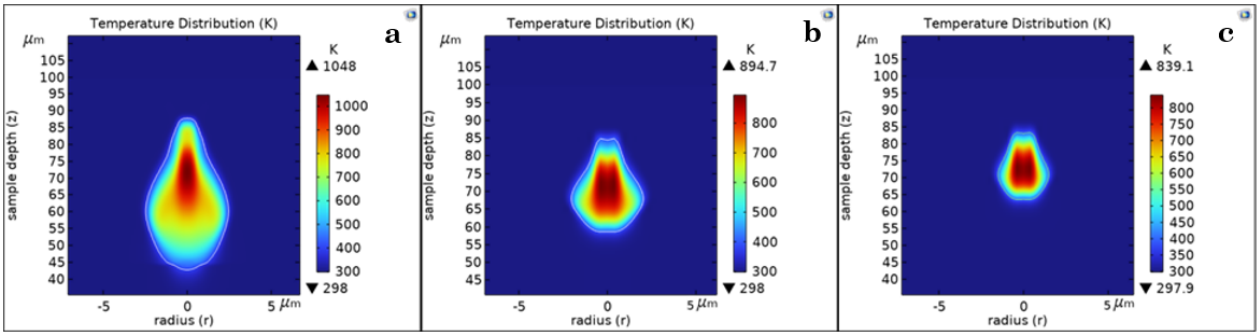

Figure 1. Calculated initial lattice-temperature distributions produced by a 50 fs laser pulse at a wavelength of 800 nm for pulse energies of (a) 1 μJ, (b) 0.5 μJ, and (c) 0.3 μJ in bulk fused silica. The distributions correspond to the state after the deposited electronic energy has been transferred to the lattice.

1:5, and the contour (ellipse) shown in the figures is drawn to indicate a temperature of 400 K. Based on the focal geometry of the beam in the bulk of fused silica, the resulting temperature distribution is expected to be elliptical, with a radius of 1 μm and a Rayleigh length of 11.2 μm. However, as shown in Fig. 1(a), the temperature distribution takes the form of a teardrop for a pulse energy of 1 μJ. This asymmetric temperature distribution is due to nonlinear effects such as plasma defocusing and self-focusing.

b) Comparison of thermal accumulation for different repetition rates at the same time interval

Figures 2-4 compare the temporal evolution of the temperature field at a pulse energy of 300 nJ under three irradiation conditions: 1000 pulses at 1 MHz, 100 pulses at 100 kHz, and 1000 pulses at 100 kHz, respectively.

For the 1 MHz case, shown in Fig. 2, the initially confined temperature field progressively evolves into a more axisymmetric and spatially expanded distribution. As evident in Fig. 2(d), the heat-affected region begins to acquire a rounded morphology during the early stages of irradiation, indicating the onset of pronounced pulse-to-pulse thermal accumulation. With a further increase in the number of incident pulses, the lateral extent of the temperature field continues to grow. By the end of the 1000th pulse, as shown in Fig. 2(l), the radius of the thermally affected region reaches approximately 80 μm, while the maximum temperature rises to 12,650 K. This substantial increase in both the spatial extent and peak temperature confirms the strong cumulative heating effect induced by the high repetition rate.

In Figures 2 and 3, the resulting thermal distributions at two different repetition rates, 1 MHz and 100 kHz, respectively, and a pulse energy of 300 nJ are examined. As can be seen, over the same time interval, a lower repetition rate produces a smaller heat-affected region, which may favor the formation of narrower modified tracks. Fig. 3 illustrates the thermal accumulation at a pulse energy of 0.3 μJ and a repetition rate of 100 kHz after 100 incident pulses, corresponding to the same irradiation duration considered for the 1 MHz case. A notable feature of these temperature maps is that the 1800 K contour does not appear even after the 100th pulse. Moreover, the 1400 K contour emerges only after the 90th incident pulse, as shown in Fig. 3(k), and remains confined to a very small region with a characteristic size of approximately 1 μm. This indicates that, under this combination of processing parameters, the high-temperature region remains highly localized, thereby minimizing undesired thermal effects.

A comparison between Fig. 2(c) and Fig. 3(l), which correspond to the thermal distributions after 100 pulses at repetition rates of 1 MHz and 100 kHz, respectively,

shows that reducing the repetition rate significantly decreases the spatial extent of the temperature field. Furthermore, comparing Fig. 2(l) and Fig. 3(l), which represent the thermal distributions after the same irradiation time of 1000 μs, confirms that the higher repetition rate produces a broader heat-affected region. This comparison demonstrates that thermal accumulation is substantially more pronounced at 1 MHz than at 100 kHz.

Fig. 4 presents the thermal accumulation behavior at a pulse energy of 0.3 μJ and a repetition rate of 100 kHz for 1000 incident pulses. Comparing the size and evolution of the temperature distribution at the end of the 1000th pulse with the corresponding case at 1 MHz, shown in Fig. 2, reveals that even after 1000 pulses, the thermal accumulation in Fig. 4(l) expands the 1400 K contour to a diameter of only approximately 20 μm, while the 1800 K contour reaches a diameter of about 3 μm. In addition, the peak temperature at the end of the 1000th pulse for the 100 kHz case is only 1864 K.

Therefore, at a repetition rate of 100 kHz, thermal accumulation leads to a temperature distribution whose dimensions remain very close to those of the focal geometry. Moreover, the peak temperature remains close to the melting temperature of glass. Compared with the response obtained at 1 MHz for the same number of pulses, shown in Fig. 2(l), no excessive temperature rise is observed in the 100 kHz case.

c) Investigating thermal accumulation for different repetition rates

We then examine the effect of varying repetition rates on thermal accumulation in a stationary fused silica sample. Fig. 5 illustrates thermal accumulation as a function of the number of pulses delivered during a sequence of 12 pulses, with repetition rates ranging from 1 kHz to 1 MHz. The data indicate that, at a pulse energy of 1 μJ and a pulse duration of 50 fs, significant thermal accumulation is not observed at repetition rates of 1, 5, and 10 kHz. However, at a repetition rate of 20 kHz, by the end of the 12th pulse, the thermal probe registers a temperature increase of approximately 100 K above ambient temperature at the center of the thermal distribution produced by the pulse. This accumulation increases with higher repetition rates; at 100 kHz, the temperature increase reaches 200 K by the 12th pulse, at 400 kHz it rises to 800 K, and at 1 MHz, it reaches 1400 K. Because the sample remains stationary and the pulses are consistently incident on the same point, increasing the repetition rate decreases the interval between consecutive pulses, thereby enhancing thermal accumulation.

Fig. 5 highlights two important temperatures of fused silica-the melting and annealing temperatures. It is crucial to note that the annealing temperature range is lower than the temperature at which the glass starts to soften or melt. Annealing is a process that involves heating the glass sample below its melting point and then cooling it to improve its durability. The glass remains rigid within the annealing temperature range and does not soften.

The annealing range is associated with structural relaxation of the glass network and a reduction in residual stress. If the material cools rapidly through the strain range, structural relaxation becomes limited and residual stresses may remain. Repeated heating below the softening or melting range may therefore influence the local stress state, whereas repeated melting may enlarge the heat-affected region and produce unwanted thermal effects.

In fused silica, the annealing temperature range starts at slightly below 1400 K and extends to below the melting temperature of the glass, which is 1938 K. As discussed above, repetition rates of 1, 5, and 10 kHz at a pulse energy of 1 μJ for a stationary sample produce only a small residual temperature rise over the first 12 pulses. This is because the temperature increase caused by thermal accumulation at these repetition rates does not reach the threshold of the annealing temperature range, as is clear from the figure. In fact, it is within this temperature range that strain occurs in the glass, and the resulting stresses can either remain in the sample or be removed by heat treatment.

For repetition rates of 20, 50, and 100 kHz, this threshold may be reached as a result of thermal accumulation as the number of pulses increases. Two scenarios may arise here. Thermal stability may occur within the annealing temperature range or slightly above the melting temperature of the glass. Achieving thermal stability means that, after a specific number of pulses have been incident on the sample, the temperature rise-and-fall cycle for each subsequent pulse remains within a specific temperature range and does not exceed it.

If this temperature range corresponds exactly to the annealing temperature range, such that these fluctuations remain below the melting temperature of the glass, it may lead to changes in the refractive index of the glass during annealing. In this case, the sample does not melt; rather, as a result of successive pulses, its temperature increases below the melting point and then cools to the strain point. This process is repeated within the same annealing-temperature range for each subsequent pulse. In this way, a re-annealing process occurs, which can gradually relieve the stresses created in the written line.

In the second case, repeated melting of the glass may lead to unwanted thermal effects and the formation of a larger heat-affected zone (HAZ).

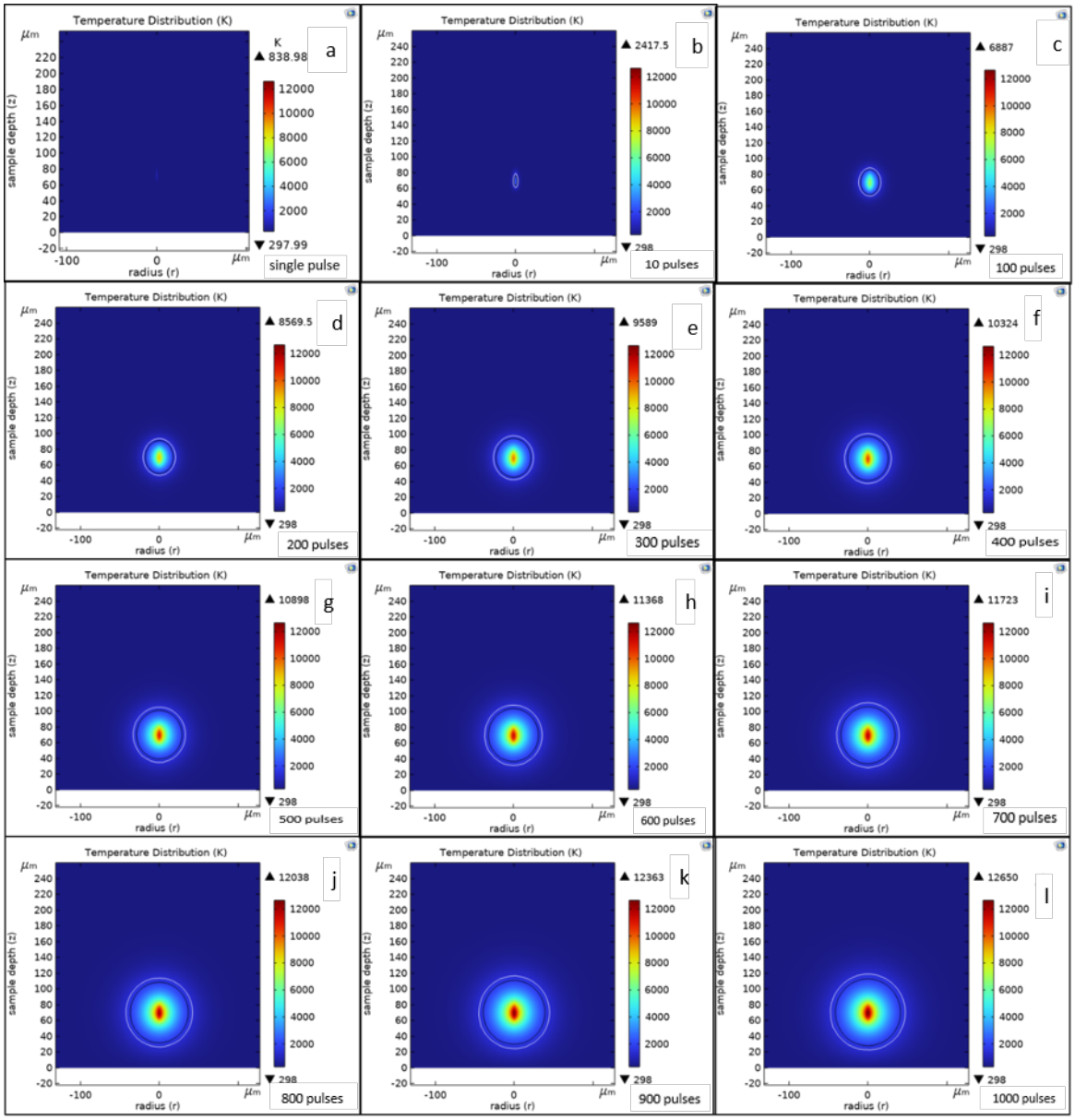

Figure 2. Evaluation of thermal accumulation in fused silica under stationary irradiation with 1000 pulses of 50 fs duration at a repetition rate of 1 MHz, obtained using the model. Temperature distributions are presented at 0, 10, 100, 200, 300, 400, 500, 600, 800, 900, and 1000 μs.

d) The role of micromachining parameters of scan speed, repetition rate, and the number of implanted pulses in achieving thermal stability

Fig. 6 illustrates the effect of scanning speeds of 10, 36, and 75 mm/s on achieving thermal stability. The results indicate that, as shown in Fig. 6, thermal stability is attained in approximately 1 millisecond at a repetition rate of 50 kHz and a scanning speed of 36 mm/s, coinciding with the melting temperature of the glass and representing a potentially suitable thermal condition for localized melting.

The effect of a scanning speed of 0.8 mm/s over 10 milliseconds at repetition rates of 50, 100, and 400 kHz is analyzed in Fig. 7. It is evident that, at a repetition rate of 100 kHz, the required energy for the scanning process is provided through thermal accumulation, enabling the glass to reach its melting point. Additionally, thermal stability is attained within only 4 milliseconds. Furthermore, it is observed that this combination of parameters does not result in excessive thermal buildup at a repetition rate of 100 kHz compared with that at 400 kHz.

The simulation results presented in Fig. 8 indicate that placing 1000 pulses at each point along the scan

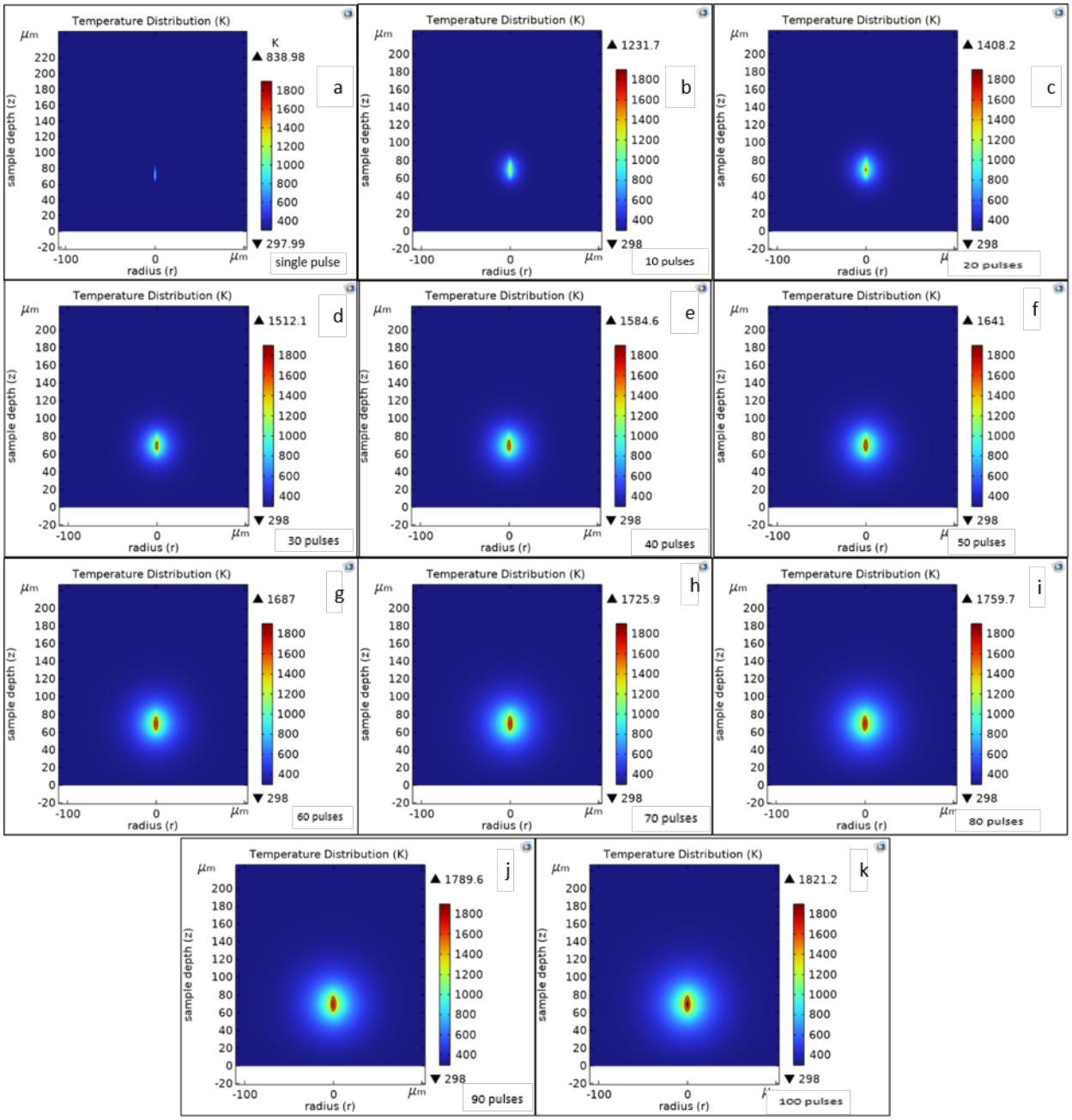

Figure 3. Thermal accumulation induced by 100 pulses with a pulse duration of 50 fs at a repetition rate of 100 kHz under stationary irradiation of the fused silica sample, calculated using the model. Temperature distributions are shown at 0, 10, 100, 200, 300, 400, 500, 600, 800, 900, and 1000 μs.

line, combined with a scanning speed of 0.8 mm/s and a repetition rate of 100 kHz, results in thermal stability with a fluctuation of 250 K around the melting point of the glass. This thermal condition may be favorable for permanent refractive-index modification.

Therefore, under different scanning speeds, when the repetition rate of the incident pulses is kept constant, higher scanning speeds result in faster thermal stabilization and lower temperatures. At different pulse repetition rates, when the scanning speed is kept constant, higher repetition rates result in greater thermal accumulation, and thermal stability is reached at a higher temperature and over a longer period.

At different repetition rates and scanning speeds, when the number of incident pulses at each point is kept constant, thermal stability is reached faster and at a higher temperature at higher scanning speeds and repetition rates. Under these conditions, thermal accumulation

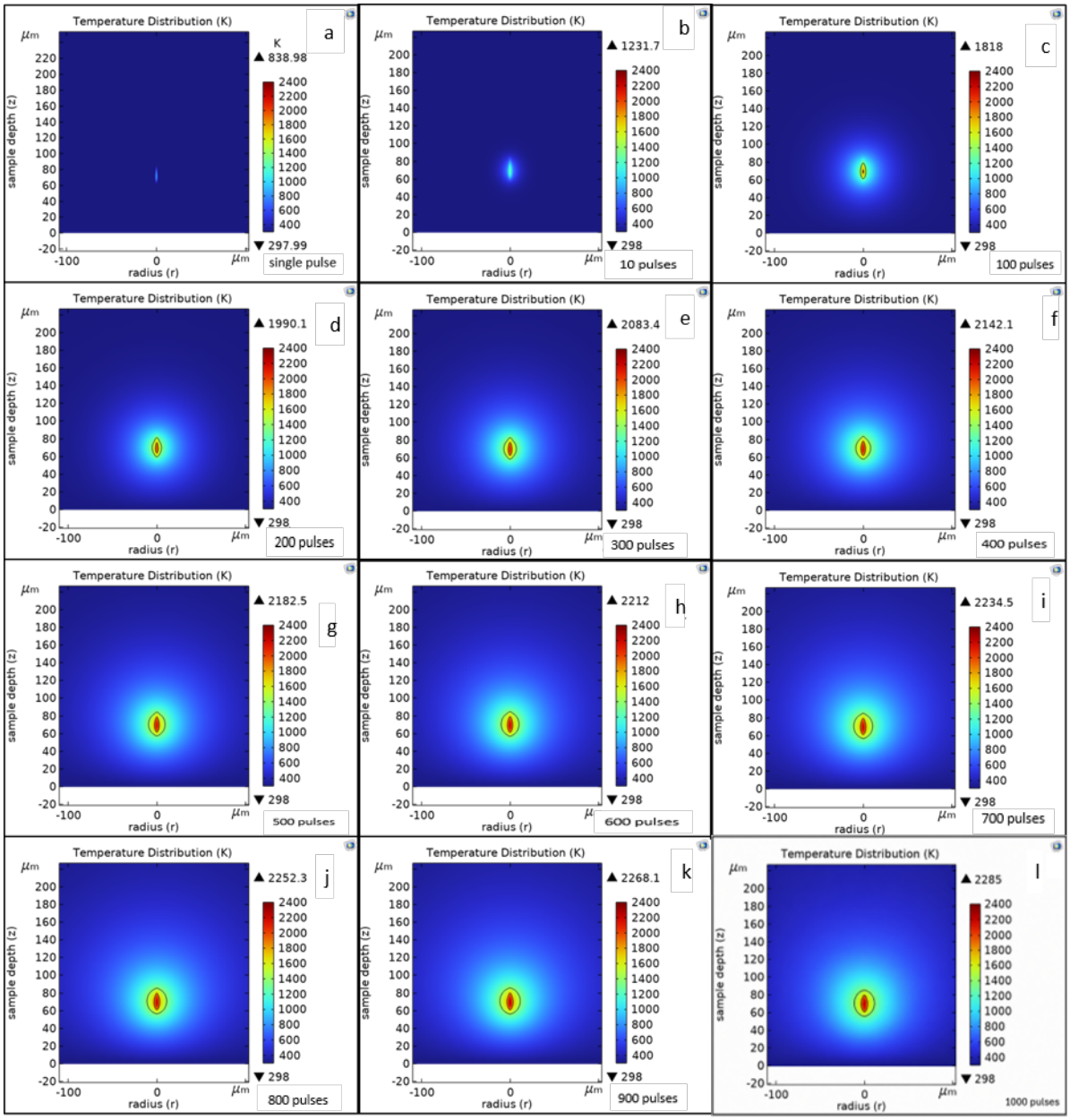

Figure 4. Thermal accumulation induced by 1000 pulses (50 fs pulse duration) at a repetition rate of 100 kHz under stationary irradiation of the fused silica sample, obtained using the model. Temperature distributions are shown at 0, 100, 1000, 2000, 3000, 4000, 5000, 6000, 8000, 9000, and 10,000 μs.

is greater, even though the scanning speed is increased proportionally with the repetition rate, than in cases with lower scanning speeds and repetition rates.

4. Conclusion

In this paper, we investigated the thermal distribution within the focal region during the interaction of ultrashort laser pulses with a transparent dielectric solid under various micromachining parameters and during laser scanning. Among the eight primary parameters, three-pulse energy, scanning speed, and repetition rate-were studied while the wavelength, pulse duration, and focusing conditions were kept constant. To calculate the temperature distribution produced by a single femtosecond pulse, the coupled nonlinear Schrodinger and plasma evolution equations were solved to obtain the deposited energy density within the material. The influence of pulse energy on the thermal distribution was then examined. Higher pulse energies resulted in higher temperature peaks, broader spatial distributions, and the

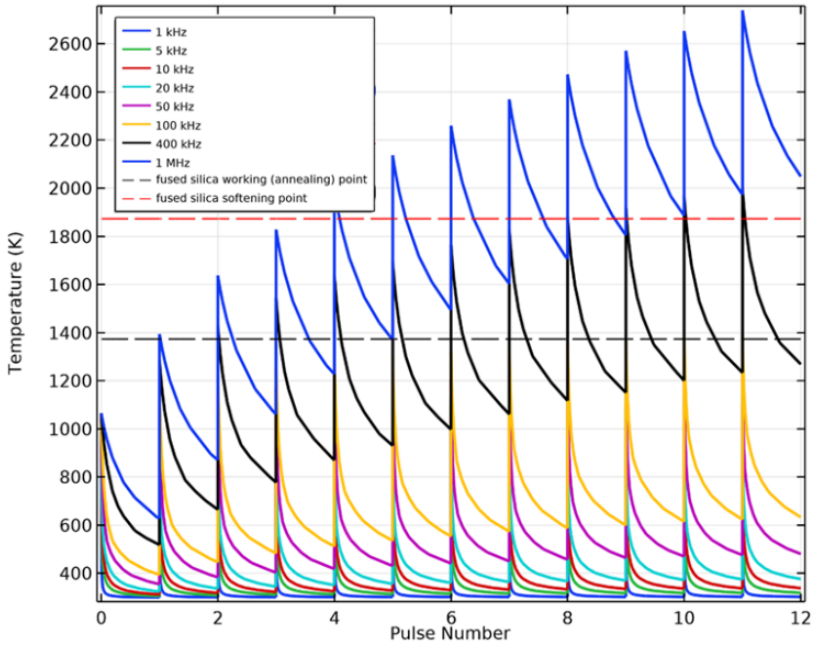

Figure 5. Investigation of the effect of thermal accumulation from a 50 fs pulse with an energy of 1 μJ at repetition rates of 1, 5, 10, 20, 50, 100, and 400 kHz, and 1 MHz within fused silica. The black and red dashed lines represent the critical points corresponding to the onset of the annealing zone and the melting point of fused silica, respectively.

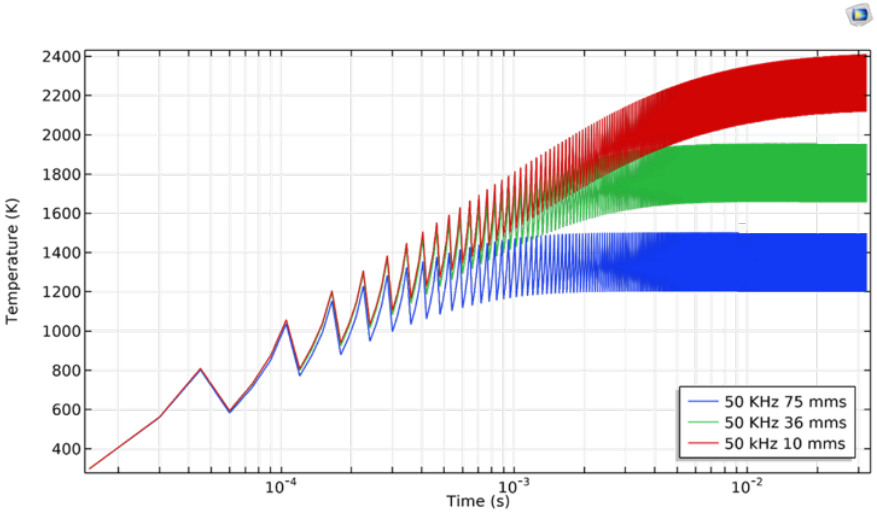

Figure 6. Examination and comparison of temperature changes along the scanning path and the time required to reach thermal stability at a fixed repetition rate of 50 kHz and for different scanning speeds of 75 (blue), 36 (green), and 10 (red) mm/s, shown in a semi-logarithmic plot of temperature versus time.

appearance of lateral lobes at shallower depths. As the pulse energy increased, the geometry of the distribution deviated further from the ellipsoidal focal volume.

Next, by solving the non-Fourier heat-diffusion equation for the resulting temperature distributions, it was observed that higher pulse energies led to longer cooling times within the focal region and its surroundings due to higher temperature peaks and steeper thermal gradients. Moreover, the initial shape of the thermal distribution significantly affected its evolution. At higher pulse energies, the diffused heat became more elongated and elliptical and spread over a volume larger than the focal region, whereas at lower energies, the final distribution became rounder and more symmetric.

Further analysis of identical pulse energies at repetition rates of 100 kHz and 1 MHz in a stationary sample revealed that, over equal time intervals, the accumulated thermal distribution at higher repetition rates became rounder and more symmetric. However, the diameter of the thermally affected region increased substantially

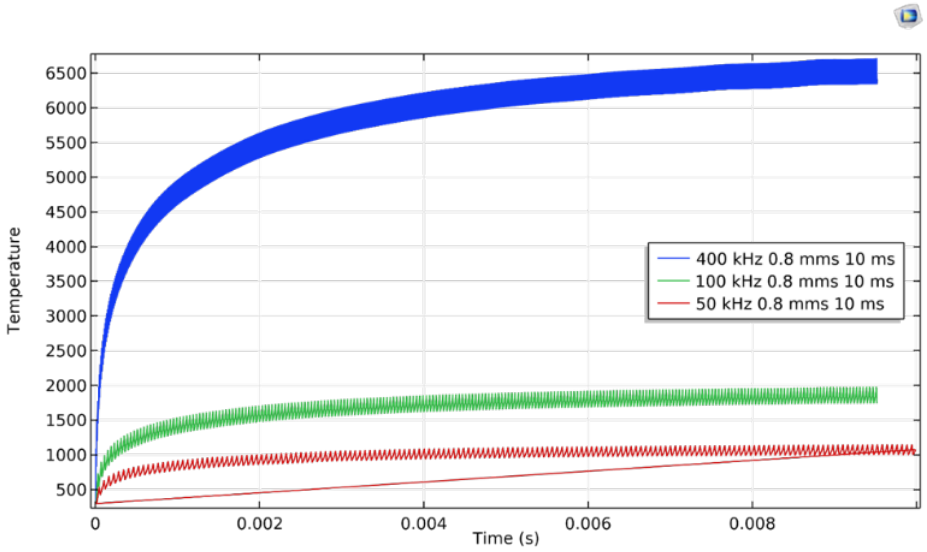

Figure 7. Examination and comparison of the time evolution of the maximum temperature during scanning at a constant scanning speed of 800 μm/s and for different repetition rates of 400 (blue), 100 (green), and 50 (red) kHz.

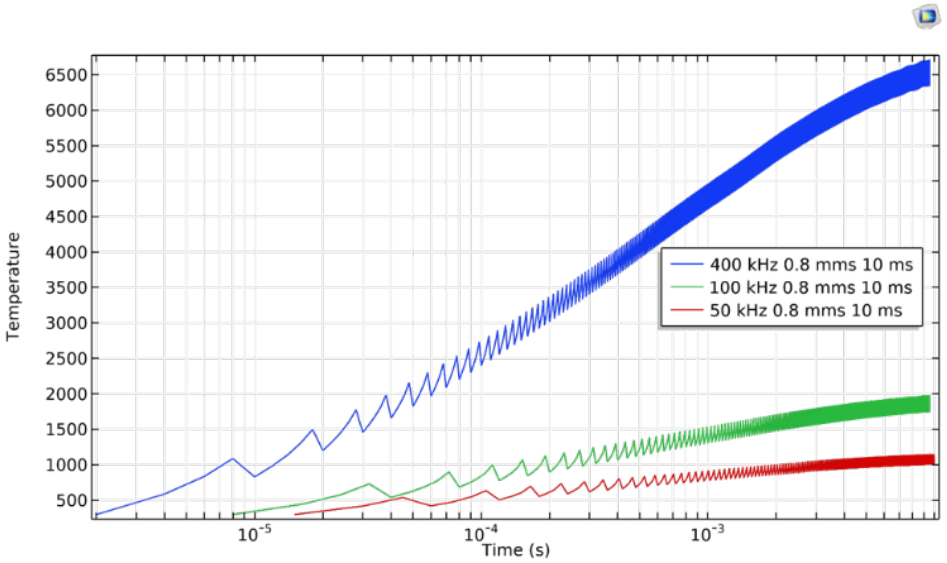

Figure 8. Examination and comparison of the time evolution of the maximum temperature during scanning at a fixed scanning speed of 800 μm/s and for different repetition rates of 400 (blue), 100 (green), and 50 (red) kHz over a scan period of 10 milliseconds. The semi-logarithmic graph of temperature is plotted against time.

beyond the focal volume at the higher repetition rate, which, if uncontrolled, may lead to undesirable thermal effects.

Under the same conditions at 100 kHz, a comparison of thermal accumulation for pulse energies of 1 μJ and 0.3 μJ showed that the higher-energy pulses produced a final accumulated thermal distribution that was rounder. However, in both cases, the spatial extent of the high-temperature region remained comparatively close to the focal volume. At different scanning speeds with a fixed pulse repetition rate, higher scanning speeds led to faster thermal stabilization and lower quasi-steady-state peak temperatures. At different pulse repetition rates with a constant scanning speed, higher repetition rates resulted in stronger thermal accumulation, higher quasi-steady-state peak temperatures, and longer times to reach thermal stability.

Finally, for various combinations of repetition rate and scanning speed, while keeping the number of pulses per point constant, higher scanning speeds and repetition rates led to faster thermal stabilization at higher temperatures. Thermal accumulation was also greater under

these conditions, even though the scanning speed was increased proportionally with the repetition rate.

References

[1] L. Huang, "Fabrication and characterization of ultrafast direct laser written waveguides," D.Phil. thesis, University of Oxford, Oxford, U.K., 2015.

[2] D. Du, X. Liu, G. Korn, J. Squier, and G. Mourou, "Laser-induced breakdown by impact ionization in SiO2 with pulse widths from 7 ns to 150 fs," Applied Physics Letters, vol. 64, no. 23, pp. 3071–3073, 1994, doi: 10.1063/1.111350.

[3] K. M. Davis, K. Miura, N. Sugimoto, and K. Hirao, "Writing waveguides in glass with a femtosecond laser," Optics Letters, vol. 21, no. 21, pp. 1729–1731, 1996, doi: 10.1364/OL.21.001729.

[4] I.-B. Sohn, M.-S. Lee, and J.-Y. Chung, "Fabrication of optical splitter and passive alignment technique with a femtosecond laser," IEEE Photonics Technology Letters, vol. 17, no. 11, pp. 2349–2351, 2005, doi: 10.1109/LPT.2005.858101.

[5] J. Liu, Z. Zhang, S. Chang, C. Flueraru, and C. P. Grover, "Directly writing of 1-to-N optical waveguide power splitters in fused silica glass using a femtosecond laser," Optics Communications, vol. 253, nos. 4–6, pp. 315–319, 2005, doi: 10.1016/j.optcom.2005.04.082.

[6] D. Grobnic, S. J. Mihailov, C. W. Smelser, M. Becker, and M. W. Rothhardt, "Femtosecond laser fabrication of Bragg gratings in borosilicate ion-exchange waveguides," IEEE Photonics Technology Letters, vol. 18, no. 13, pp. 1403–1405, 2006, doi: 10.1109/LPT.2006.877230.

[7] P. R. Herman and H. Zhang, "Ultrashort-pulsed laser direct writing of strong Bragg grating waveguides in bulk glasses," in Optical Fiber Communication Conference/National Fiber Optic Engineers Conference, OSA Technical Digest (CD). Washington, DC, USA: Optical Society of America, 2008, paper OThV4.

[8] G. D. Marshall, A. Politi, J. C. F. Matthews, P. Dekker, M. Ams, M. J. Withford, and J. L. O'Brien, "Laser written waveguide photonic quantum circuits," Optics Express, vol. 17, no. 15, pp. 12546–12554, 2009, doi: 10.1364/OE.17.012546.

[9] M. Sakakura, T. Sawano, Y. Shimotsuma, K. Miura, and K. Hirao, "Fabrication of three-dimensional 1 × 4 splitter waveguides inside a glass substrate with spatially phase modulated laser beam," Optics Express, vol. 18, no. 12, pp. 12136–12143, 2010, doi: 10.1364/OE.18.012136.

[10] G. Cerullo, "Femtosecond-laser-written optical waveguides for optical communications and biophotonic applications," in CLEO/Europe–EQEC 2009: European Conference on Lasers and Electro-Optics and the European Quantum Electronics Conference, Munich, Germany, 2009, p. 789.

[11] W. J. Reichman II, "Understanding how femtosecond laser waveguide fabrication in glasses works," Ph.D. dissertation, Graduate Group in Applied Science, University of California, Davis, CA, USA, 2006, Rep. UCRL-TH-221547.

[12] D. Homoelle, S. Wielandy, A. L. Gaeta, N. F. Borrelli, and C. Smith, "Infrared photosensitivity in silica glasses exposed to femtosecond laser pulses," Optics Letters, vol. 24, no. 18, pp. 1311–1313, 1999, doi: 10.1364/OL.24.001311.

[13] A. M. Streltsov and N. F. Borrelli, "Fabrication and analysis of a directional coupler written in glass by nanojoule femtosecond laser pulses," Optics Letters, vol. 26, no. 1, pp. 42–43, 2001, doi: 10.1364/OL.26.000042.

[14] S. Nolte, M. Will, J. Burghoff, and A. Tünnermann, "Femtosecond waveguide writing: A new avenue to three-dimensional integrated optics," Applied Physics A, vol. 77, no. 1, pp. 109–111, 2003, doi: 10.1007/s00339-003-2088-6.

[15] N. B. Muhammad, "Laser micromachining of coronary stents for medical applications," Ph.D. dissertation, School of Mechanical, Aerospace and Civil Engineering, University of Manchester, Manchester, U.K., 2012.

[16] B. Neuenschwander, B. Jaeggi, M. Schmid, A. Dommann, A. Neels, T. Bandi, and G. Hennig, "Factors controlling the incubation in the application of ps laser pulses on copper and iron surfaces," in Laser Applications in Microelectronic and Optoelectronic Manufacturing (LAMOM) XVIII, Proceedings of SPIE, vol. 8607, 2013, Art. no. 86070D, doi: 10.1117/12.2004136.

[17] C. B. Schaffer, J. F. García, and E. Mazur, "Bulk heating of transparent materials using a high-repetition-rate femtosecond laser," Applied Physics A, vol. 76, no. 3, pp. 351–354, 2003, doi: 10.1007/s00339-002-1819-4.

[18] M. Sakakura, M. Terazima, Y. Shimotsuma, K. Miura, and K. Hirao, "Heating and rapid cooling of bulk glass after photoexcitation by a focused femtosecond laser pulse," Optics Express, vol. 15, no. 25, pp. 16800–16807, 2007, doi: 10.1364/OE.15.016800.

[19] S. M. Eaton, H. Zhang, P. R. Herman, F. Yoshino, L. Shah, J. Bovatsek, and A. Y. Arai, "Heat accumulation effects in femtosecond laser-written waveguides with variable repetition rate," Optics Express, vol. 13, no. 12, pp. 4708–4716, 2005, doi: 10.1364/OPEX.13.004708.

[20] F. Zimmermann, S. Richter, S. Döring, A. Tünnermann, and S. Nolte, "Ultrastable bonding of glass with femtosecond laser bursts," Applied Optics, vol. 52, no. 6, pp. 1149–1154, 2013, doi: 10.1364/AO.52.001149.

[21] M. Sakakura, M. Shimizu, Y. Shimotsuma, K. Miura, and K. Hirao, "Temperature distribution and modification mechanism inside glass with heat accumulation during 250 kHz irradiation of femtosecond laser pulses," Applied Physics Letters, vol. 93, no. 23, Art. no. 231112, 2008, doi: 10.1063/1.3046101.

[22] Y. Kondo, K. Nouchi, T. Mitsuyu, M. Watanabe, P. G. Kazansky, and K. Hirao, "Fabrication of long-period fiber gratings by focused irradiation of infrared femtosecond laser pulses," Optics Letters, vol. 24, no. 10, pp. 646–648, 1999, doi: 10.1364/OL.24.000646.

[23] Y. Sikorski, A. A. Said, P. Bado, R. Maynard, C. Florea, and K. A. Winick, "Optical waveguide amplifier in Nd-doped glass written with near-IR femtosecond laser pulses," Electronics Letters, vol. 36, no. 3, pp. 226–227, 2000, doi: 10.1049/el:20000172.

[24] I. Miyamoto, K. Cvecek, Y. Okamoto, and M. Schmidt, "Internal modification of glass by ultrashort laser pulse and its application to micro welding," Applied Physics A, vol. 114, no. 1, pp. 187–208, 2014, doi: 10.1007/s00339-013-8115-3.

[25] H. Shen, C. Tian, and Z. Jiang, "Prediction of internal modification size in glass induced by ultrafast laser scanning," Optics Express, vol. 29, no. 14, pp. 21711–21726, 2021, doi: 10.1364/OE.430475.

[26] C. Cattaneo, "Sur une forme de l'équation de la chaleur éliminant le paradoxe d'une propagation instantanée," Comptes Rendus de l'Académie des Sciences, vol. 247, pp. 431–433, 1958.

[27] S. Najafi, A. S. Arabanian, and R. Massudi, "Comprehensive modeling of structural modification induced by a femtosecond laser pulse inside fused silica glass," Journal of Physics D: Applied Physics, vol. 49, no. 25, Art. no. 255101, 2016, doi: 10.1088/0022-3727/49/25/255101.